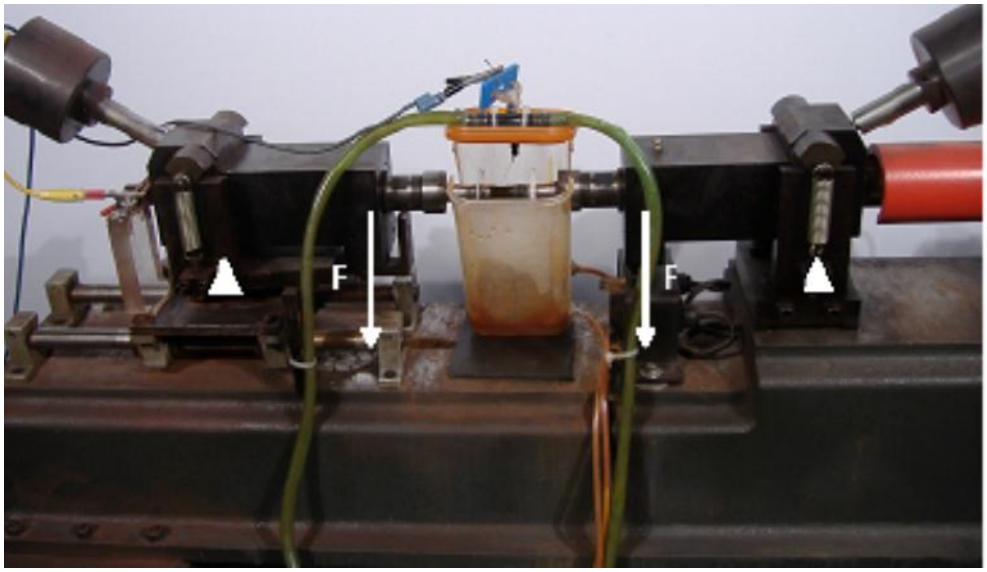

Figure 1 Apparatus for small scale corrosion fatigue tests

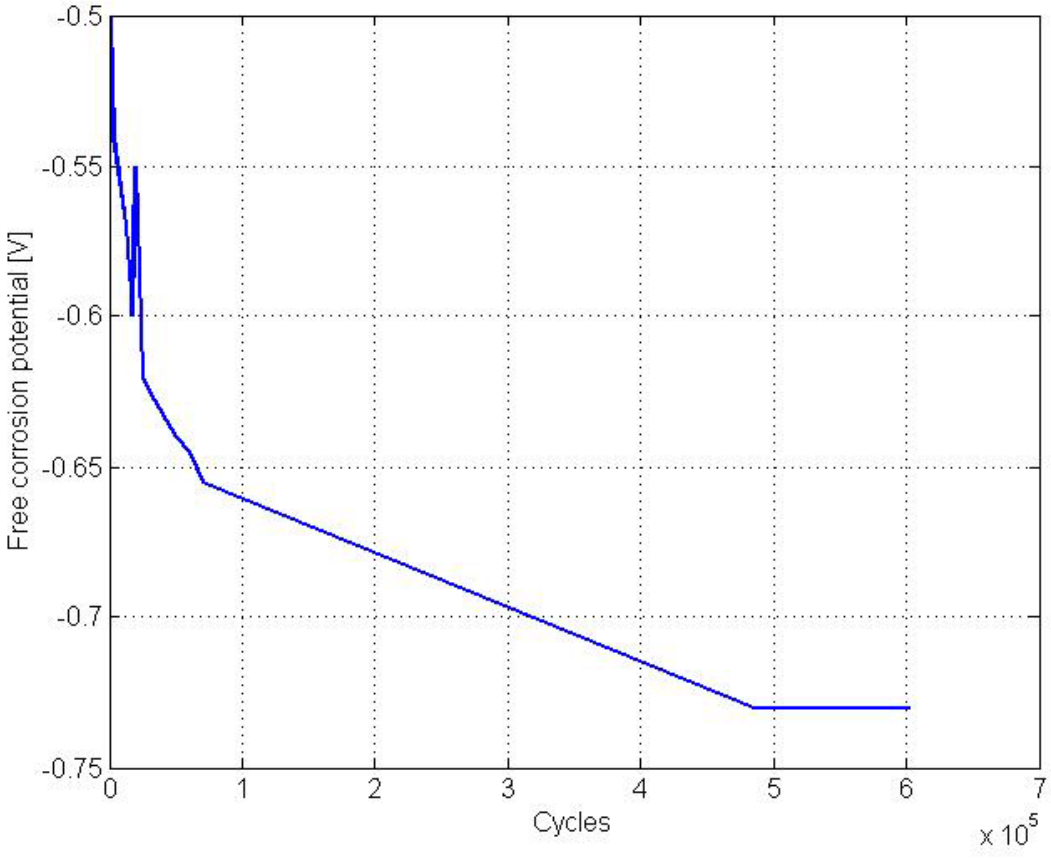

Figure 2: Free corrosion potential during the first stage of a small scale

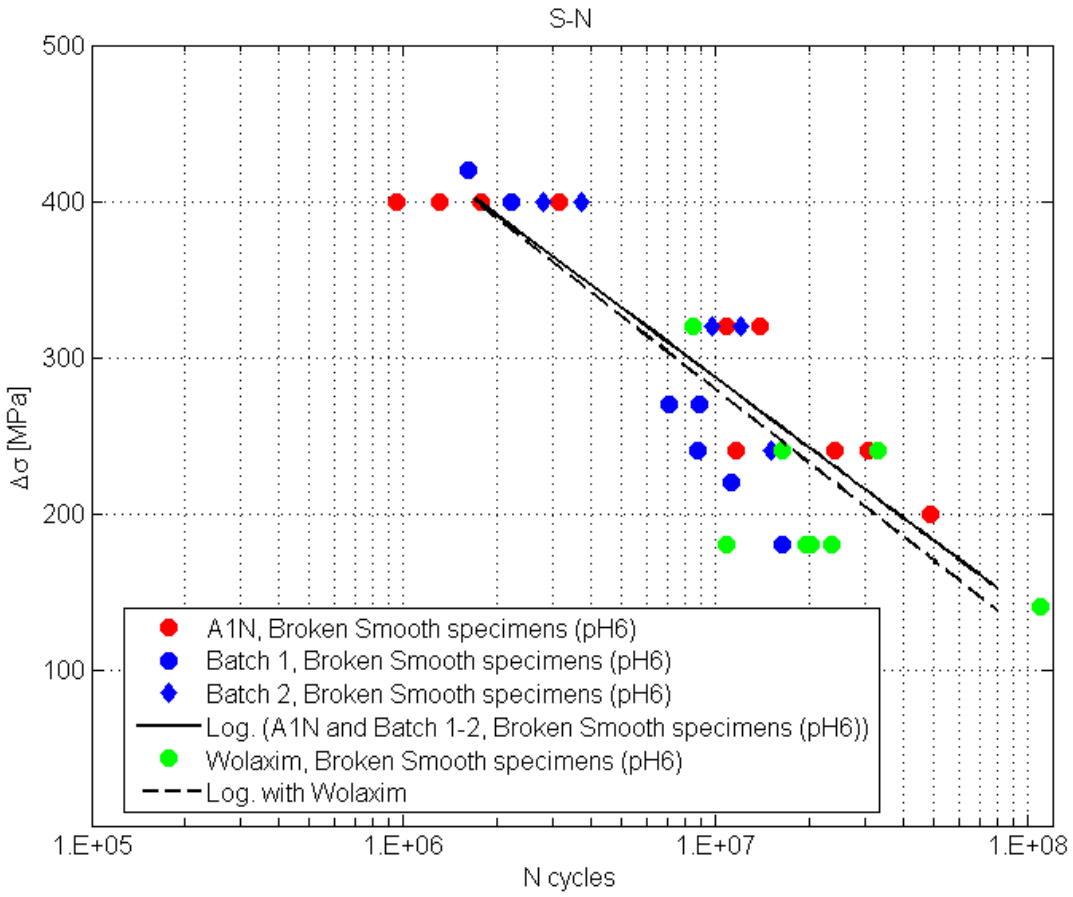

Figure 3: SN diagram for atmospheric corrosion-fatigue of A1N material.

test, A1N material.

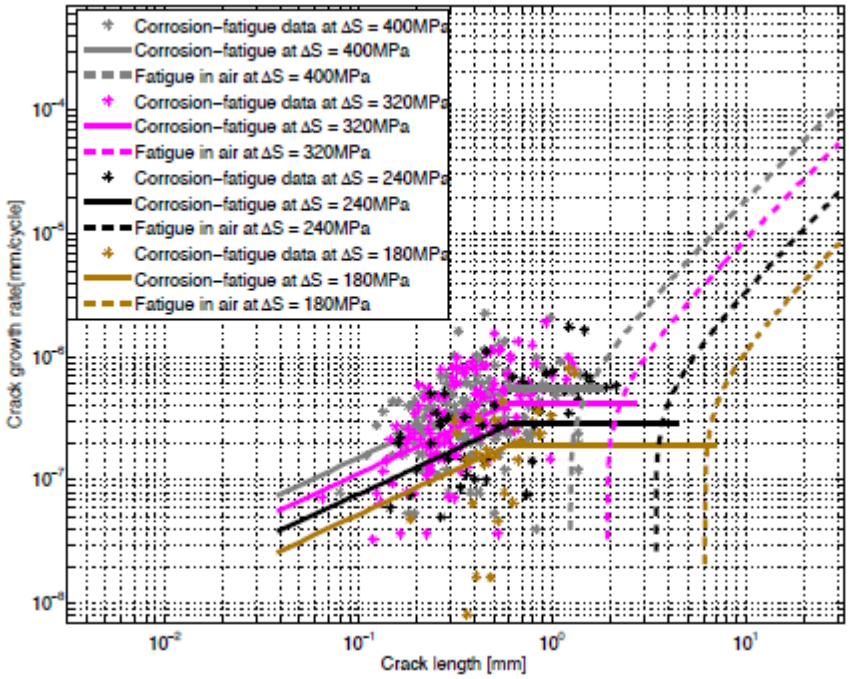

Figure 4 Wolaxim data for comparison of fatigue crack growth in air and in corrosion conditions (A4T material)

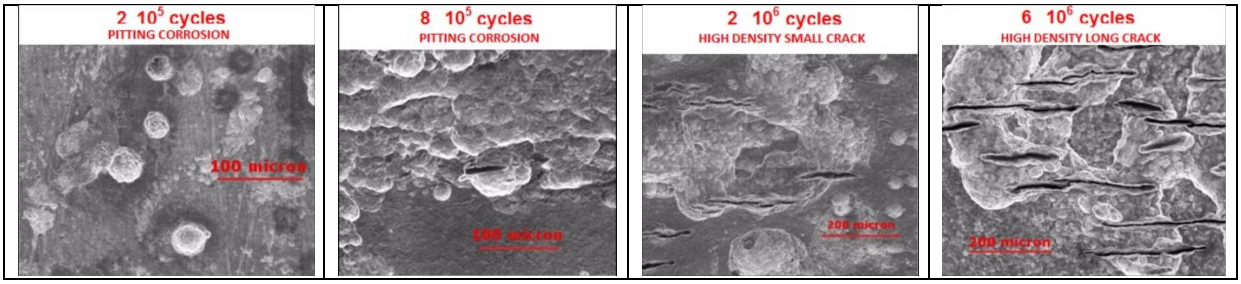

Figure 5 Stages in growth of corrosion fatigue cracks

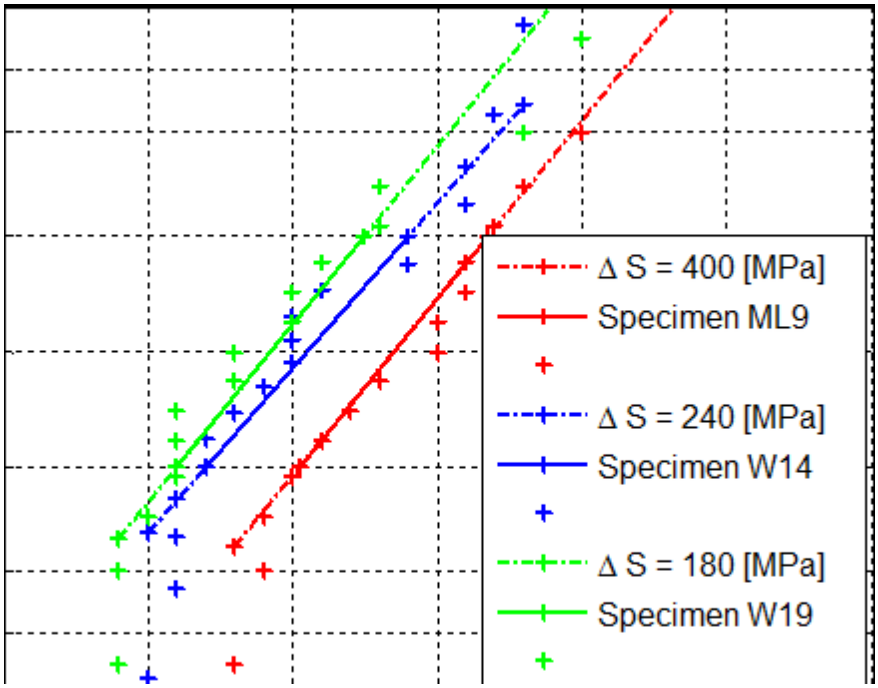

Figure 6: *Depth of the primary pit when the secondary pit appears, varying the stress level*

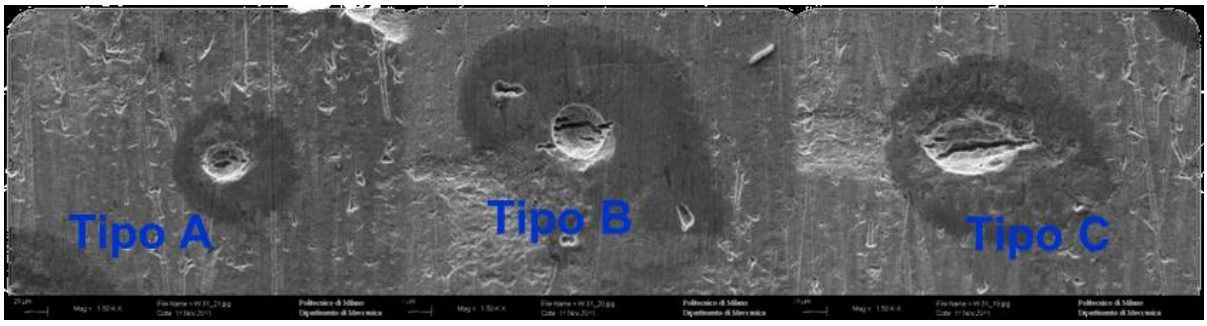

Figure 7 Growth of Crack within a pit

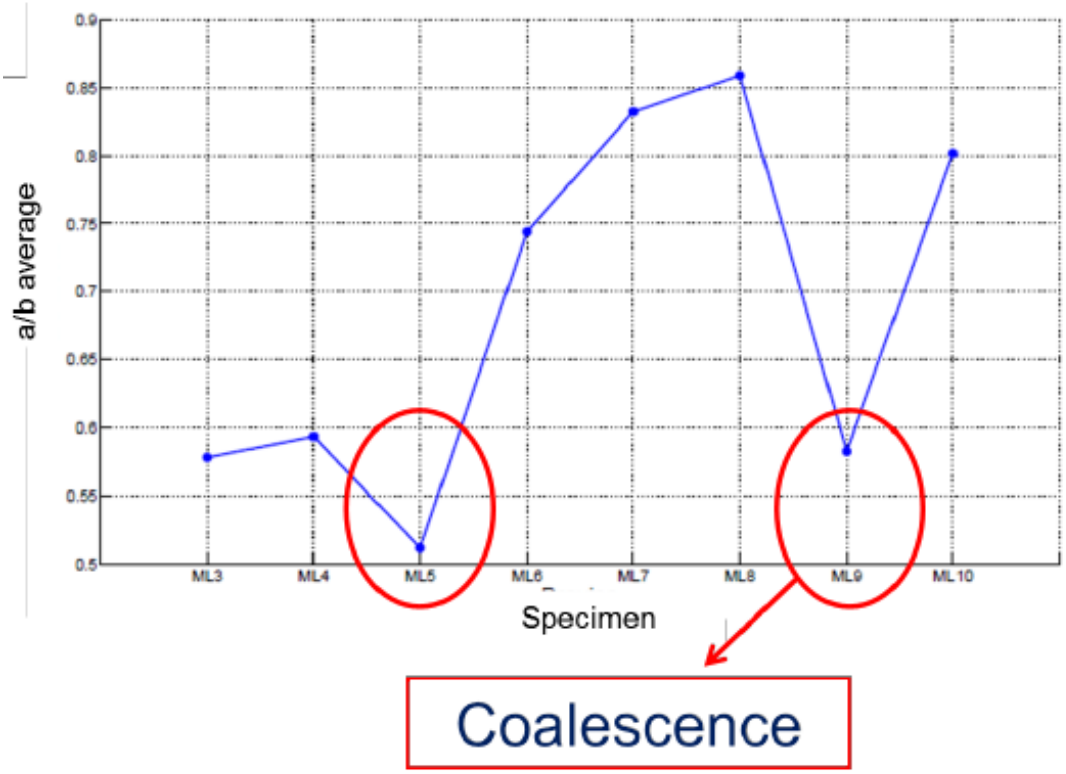

Figure 8 Aspect ratios of cracks during a fatigue test (showing coalescence)

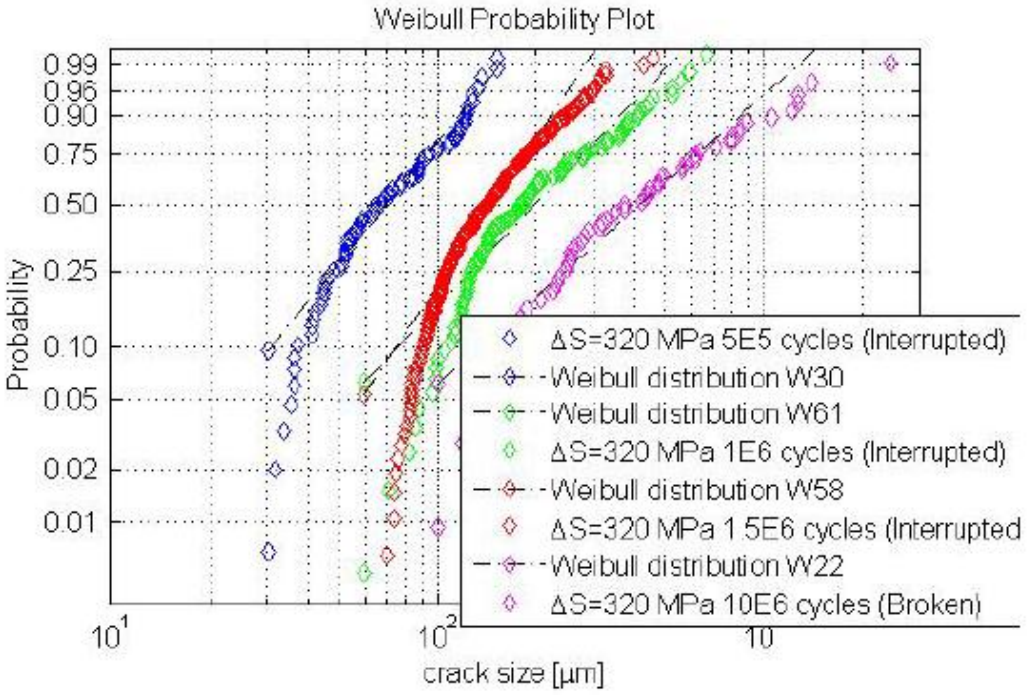

Figure 9 Crack Length Distributions for different samples

Figure 10 Microscope, holder and scanner for corrosion assessment

Figure 11 System deployed in field trials

	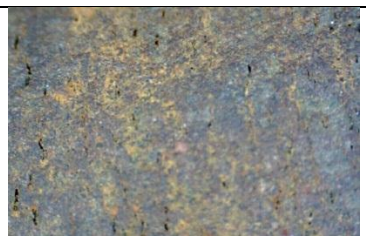	
Sample 1 (corrosion only)	Sample 2 (Small number of microcracks)	Sample 3 (large number of microcracks)

Figure 12 Examples of Images

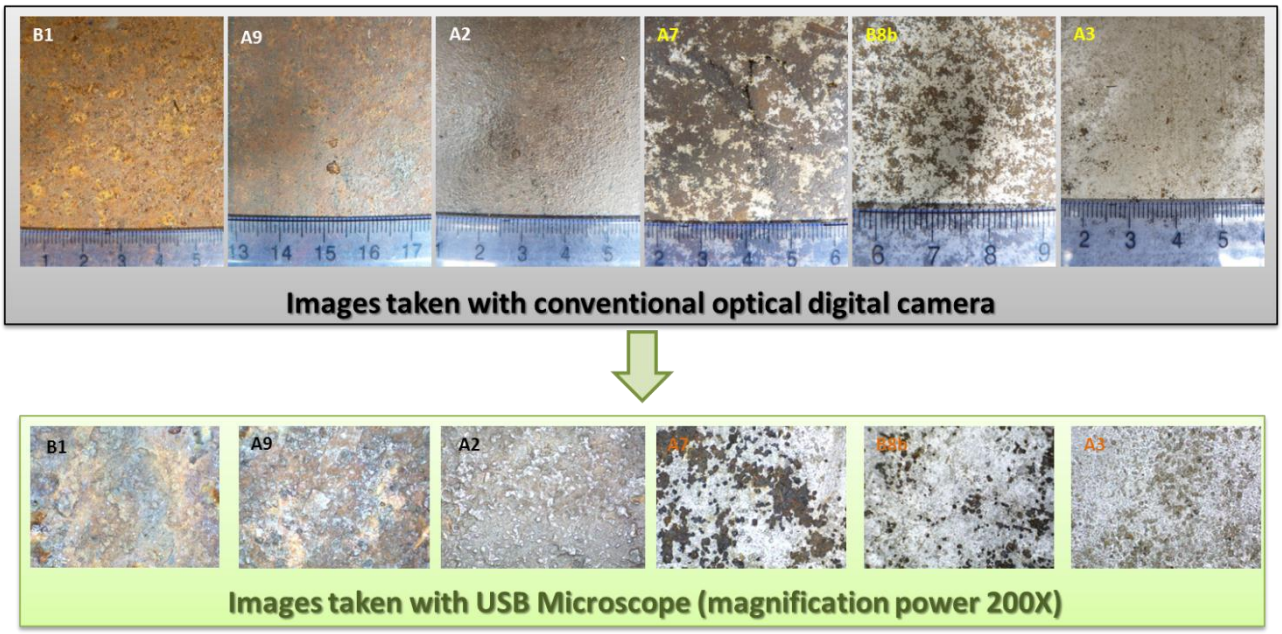

Figure 13 Effect on rusted plate of different rust removal techniques

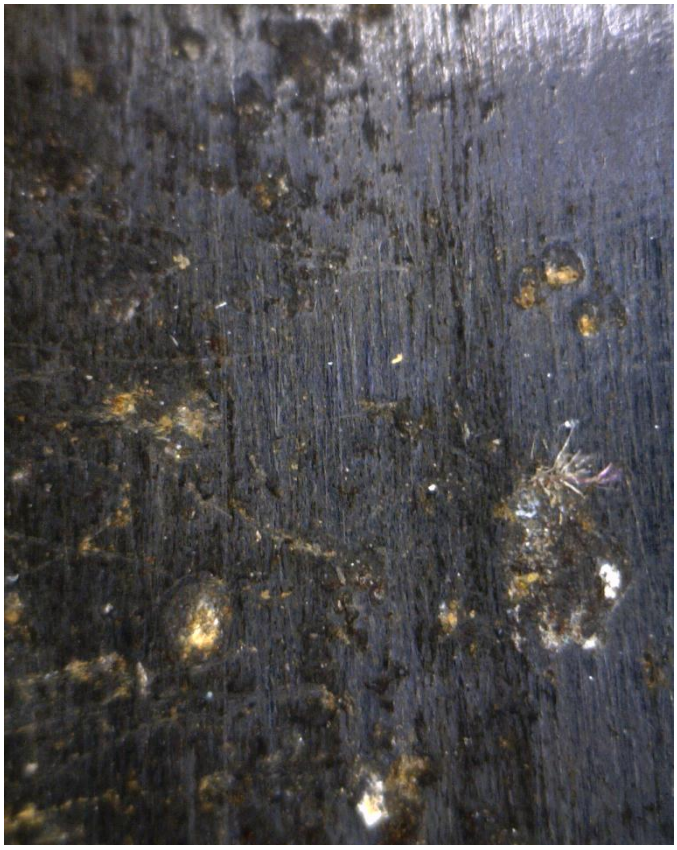

Figure 14 Scratch Marks from Abrasive Cleaning (Hamilton April 2012)

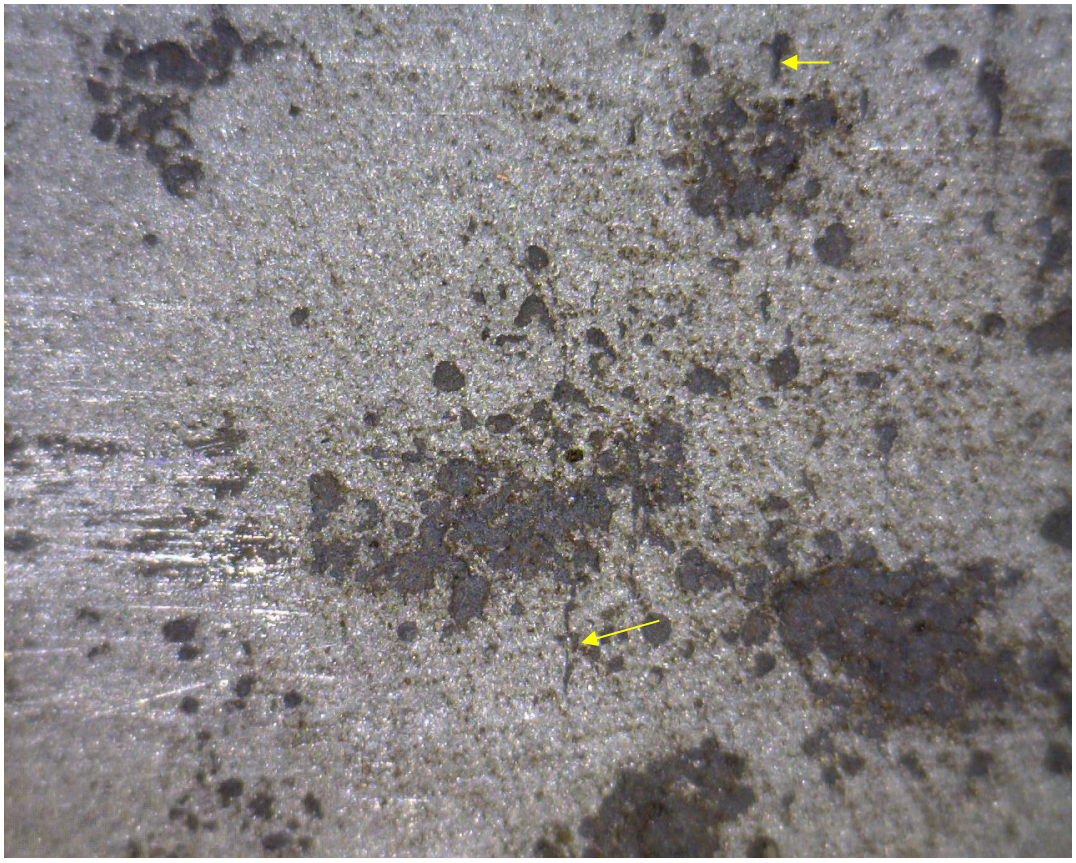

Figure 15 Example of Crack Detected

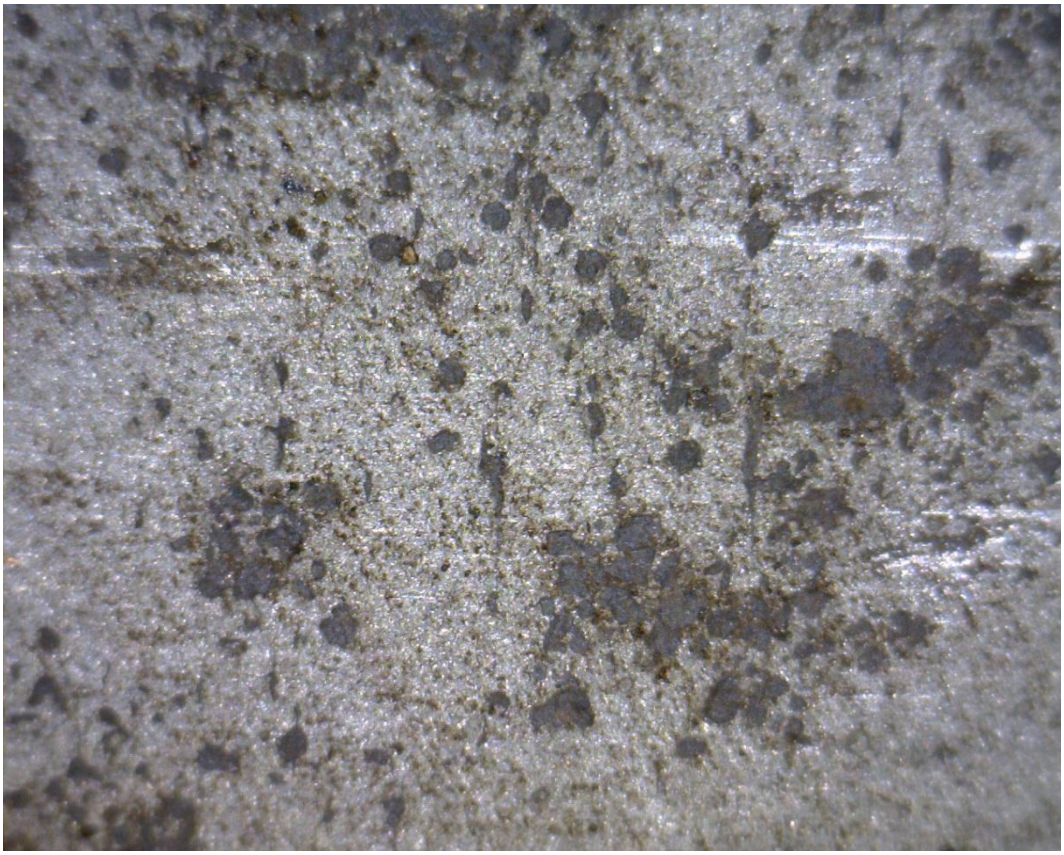

Figure 16 Example of Multiple Cracks Detected

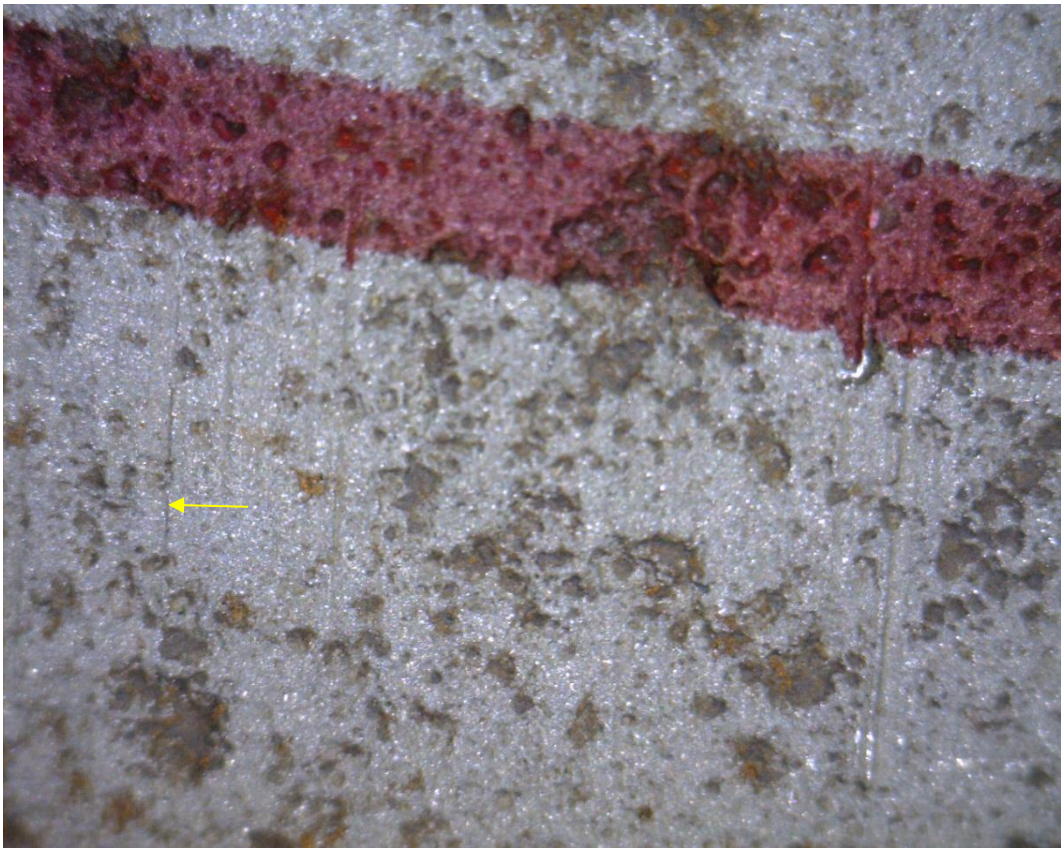

Figure 17 Example of Cracks Detected

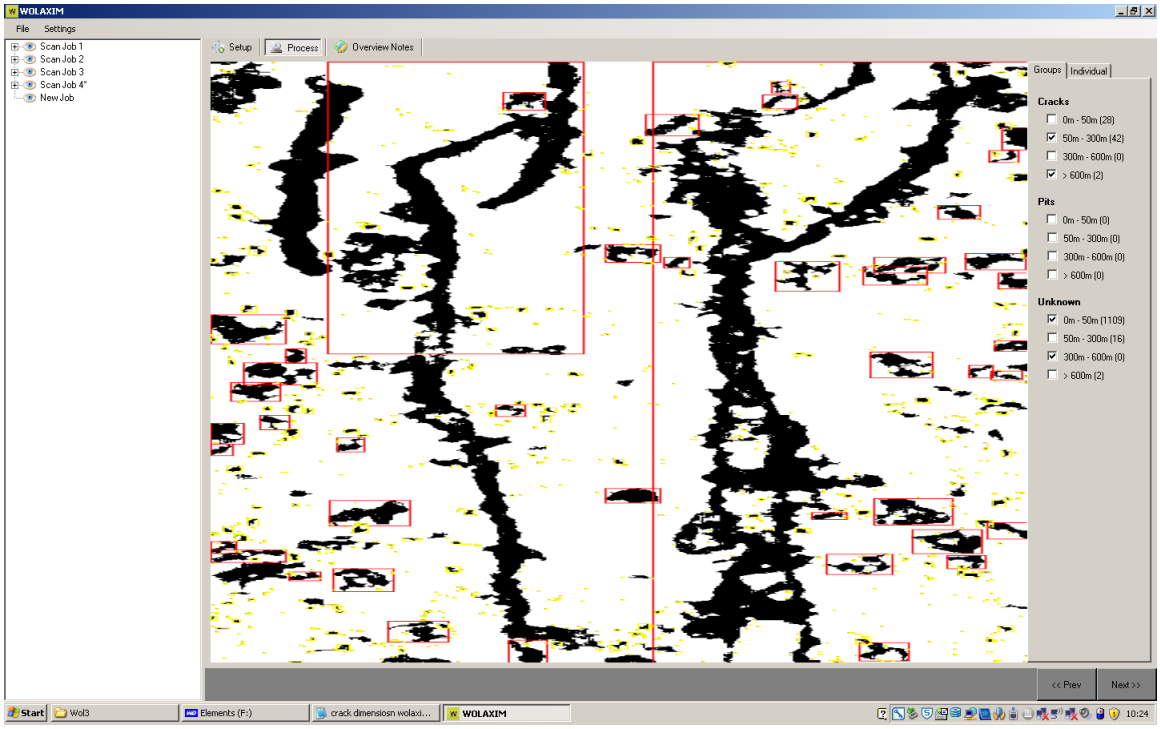

Figure 18 Software output showing crack counting

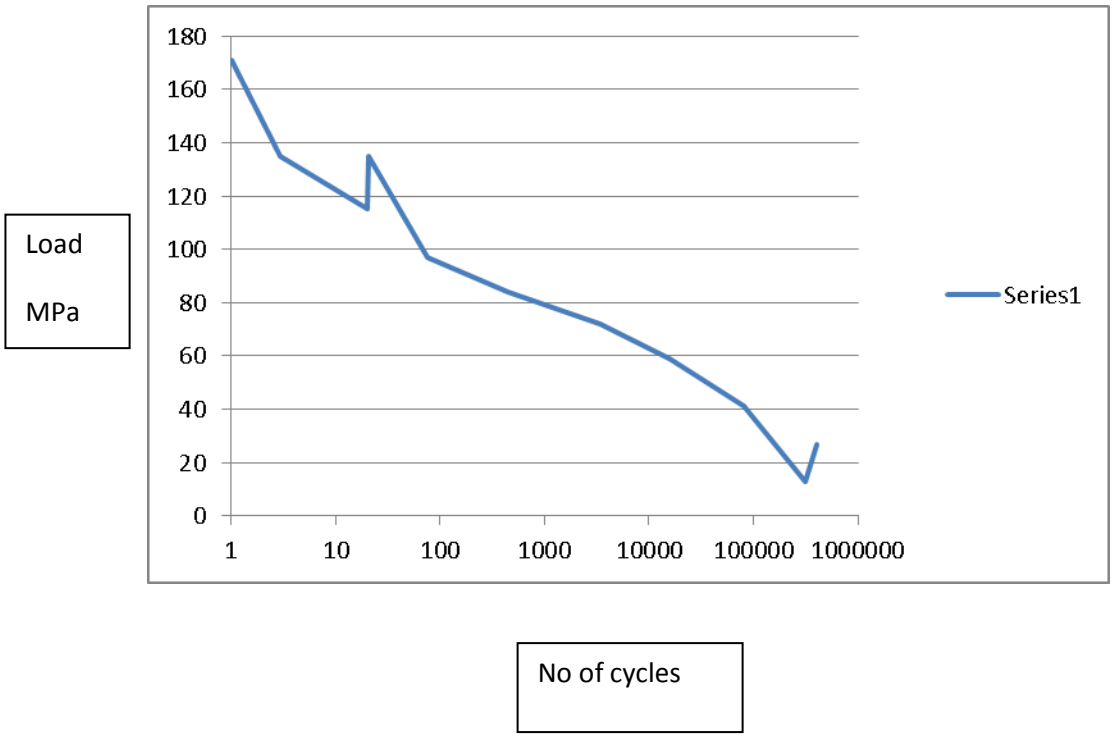

Figure 19 Load Spectrum for Case Study of Corrosion Fatigue

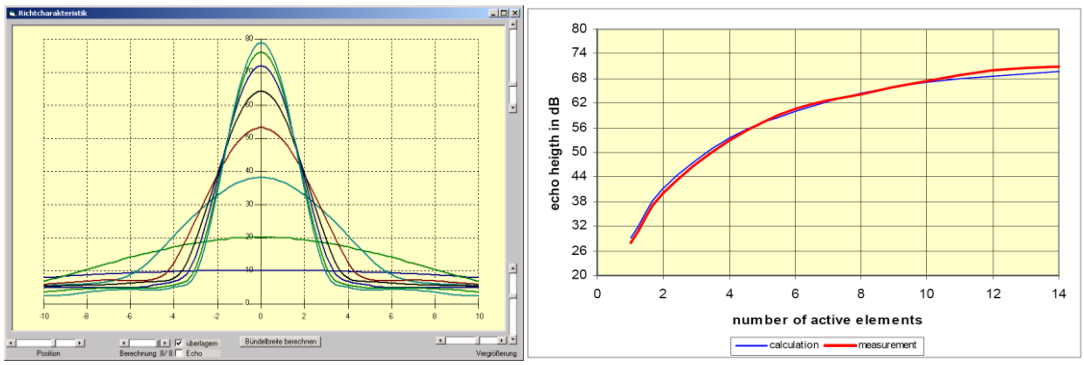

Figure 20 Modelling results for several numbers of active elements, left: circumferential directivity pattern, right: maximum echo amplitude

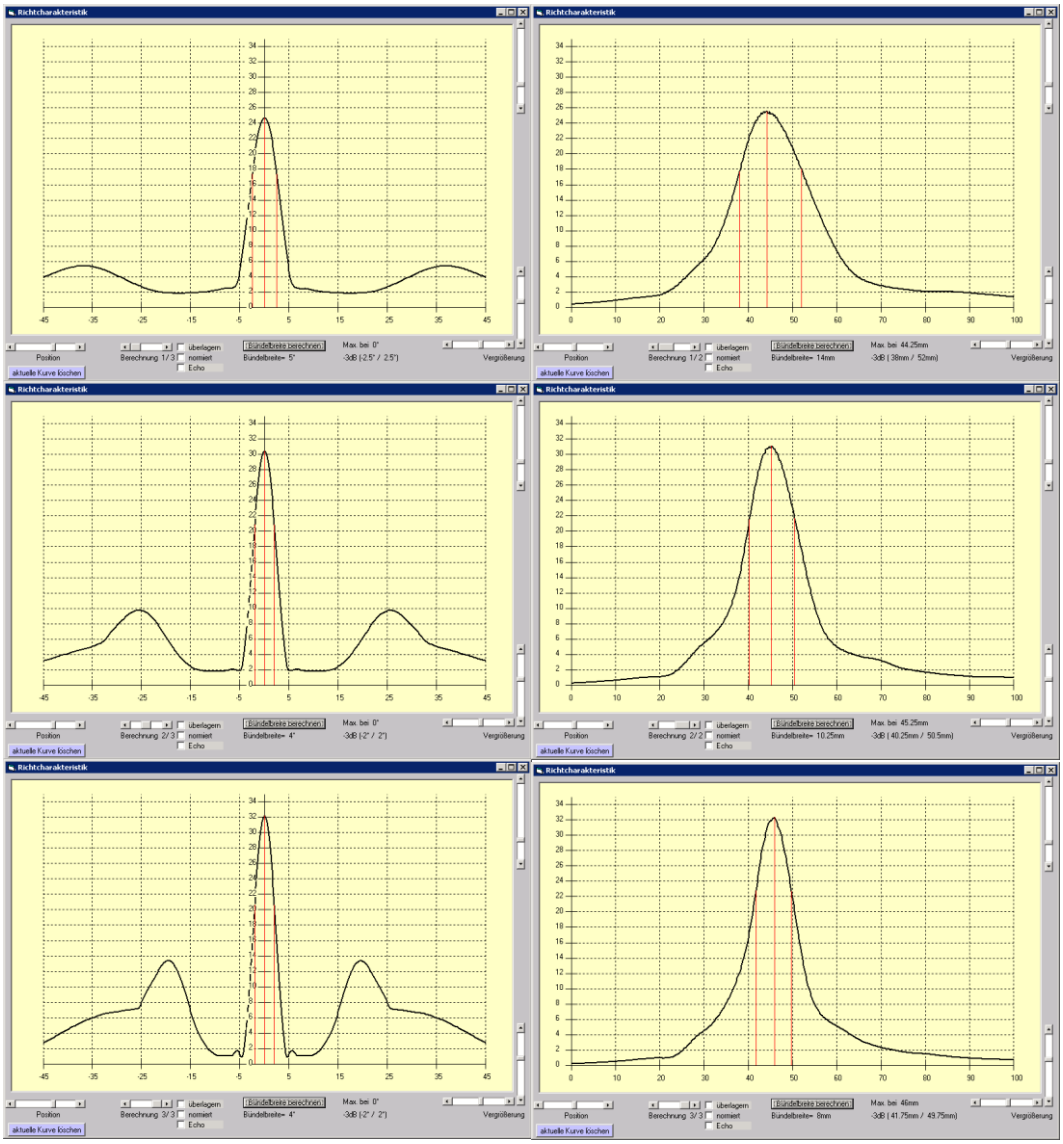

Figure 21 Modelling results, left: circumferential directivity pattern with grating lobes, right: axial directivity pattern, top: 2 MHz, middle: 3 MHz, bottom: 4 MHz

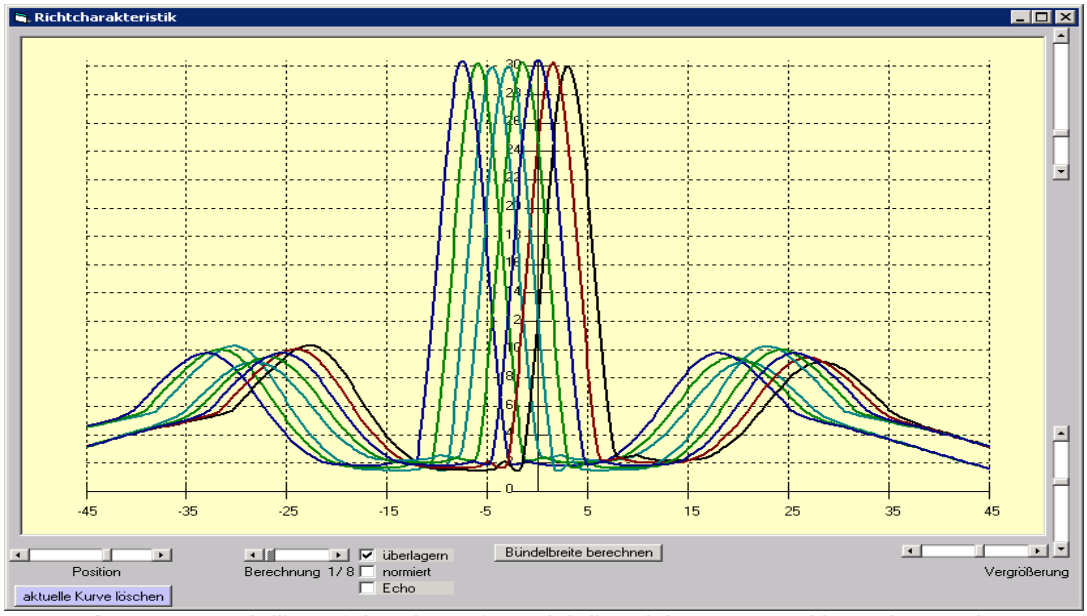

Figure 22 Modelling of the circumferential directivity pattern with angle steering

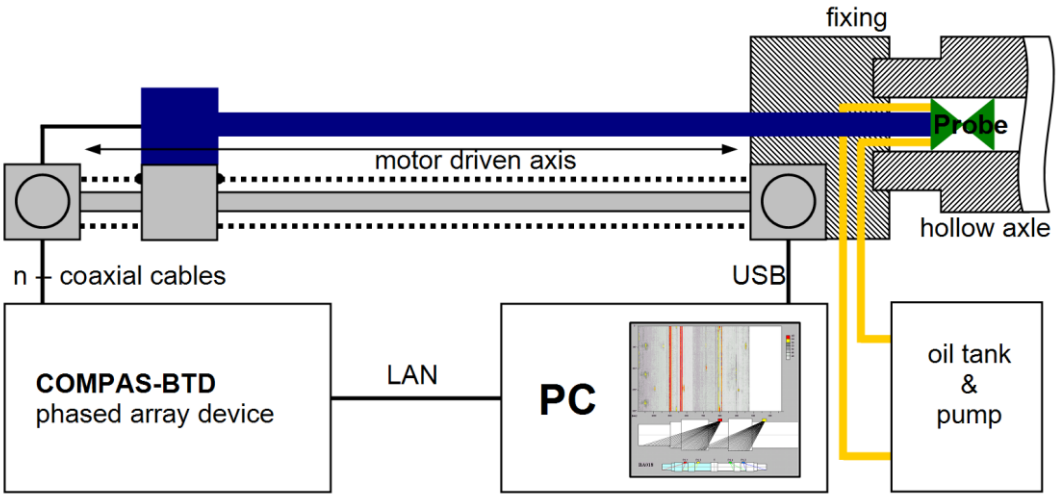

Figure 23 Concept of the ultrasonic testing system

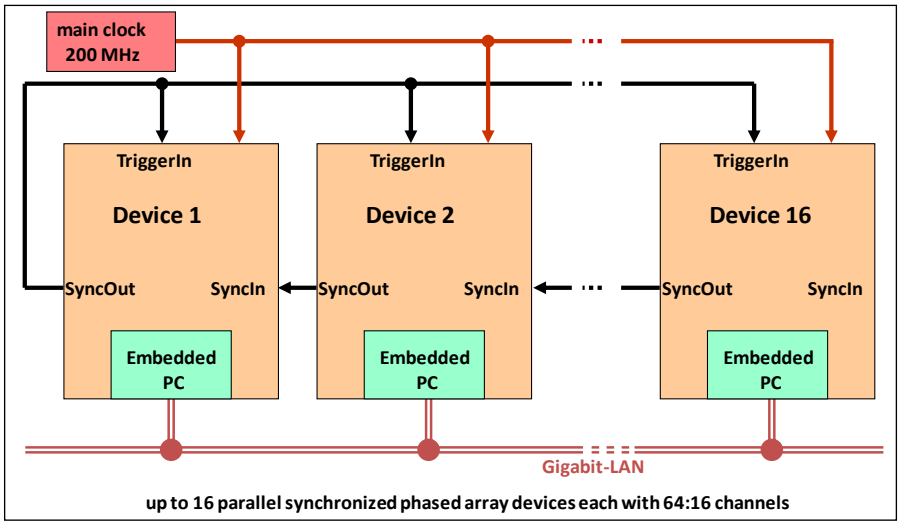

Figure 24 Principle of the parallel operation with the COMPAS phased array device

Figure 25 Phased array probe developed in project

Figure 26 Experimental Test on Test Axle

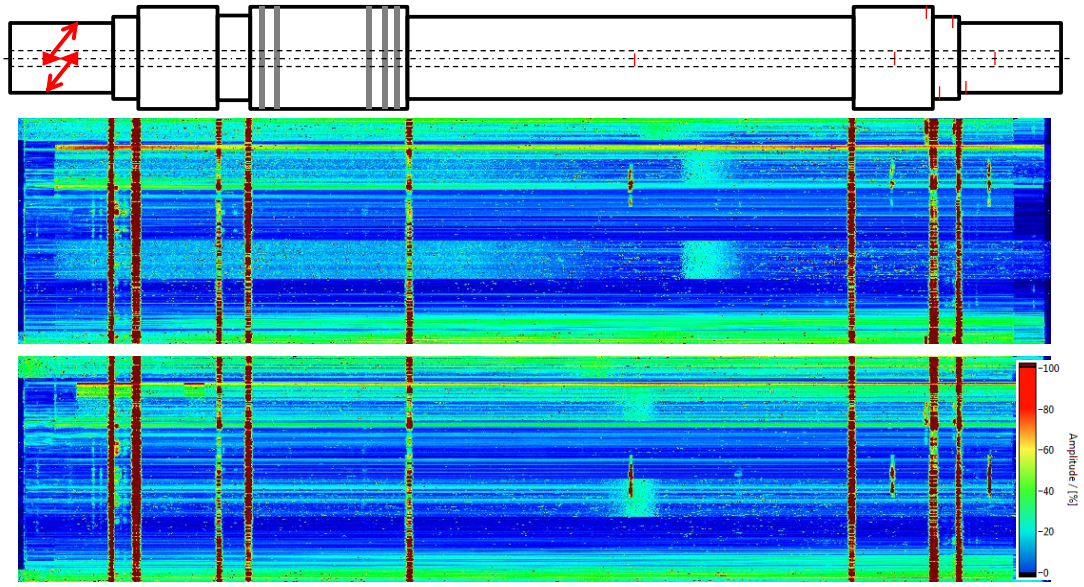

Figure 27 Results on Test Axle

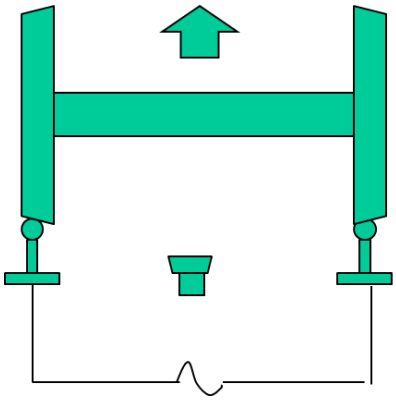

Figure 28(a) Track Mounted System

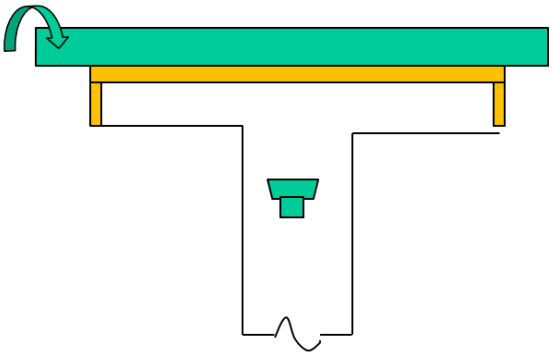

Figure 28(b) Induction System

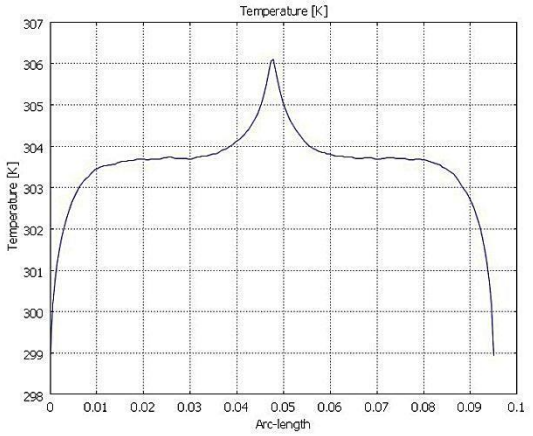

Figure 29(a) Surface Temperature with 2mm deep crack at 100KHz and 2V input (Time 3s, total horizontal scale 10cm)

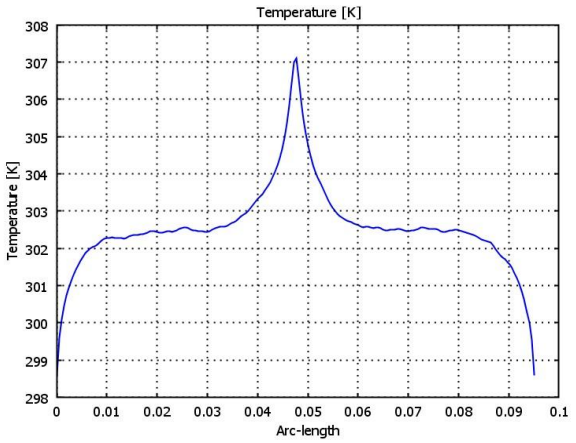

Figure 29(b) Surface Temperature with 2mm deep crack at 500KHz and 2V input (Time 3s, total horizontal scale 10cm)

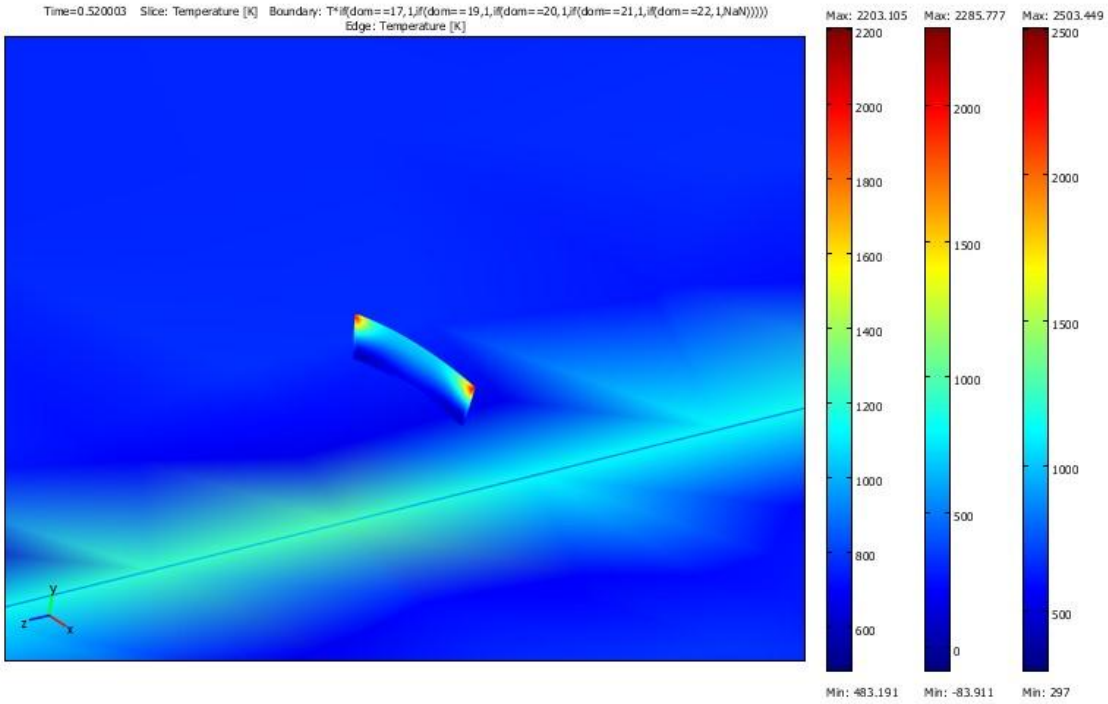

Figure 30 3D Mode; showing heating of crack ends

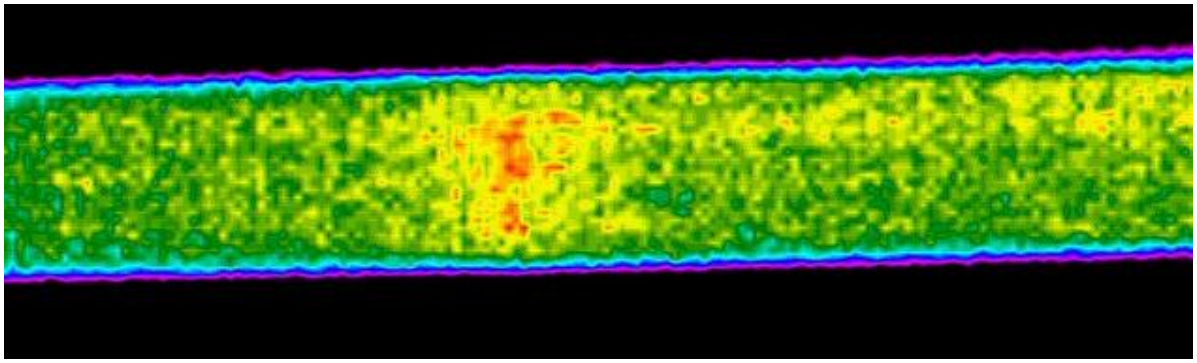

Figure 31 Image of crack in small axle at high frequency

Figure 32 3kW unit with induction loop constructed with copper pipe

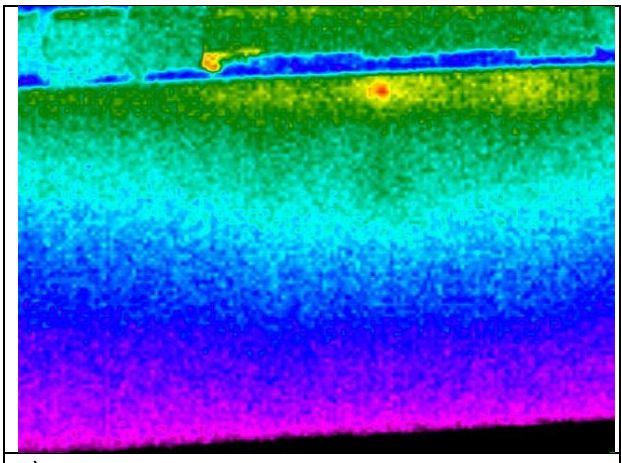

a)

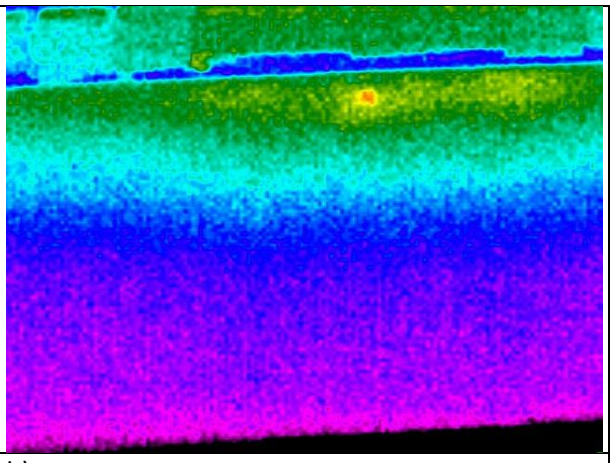

b)

Figure 33 Thermal images obtained with the roller configuration: a) image at to=0s, b) image at later time (note axle is rolling top towards camera

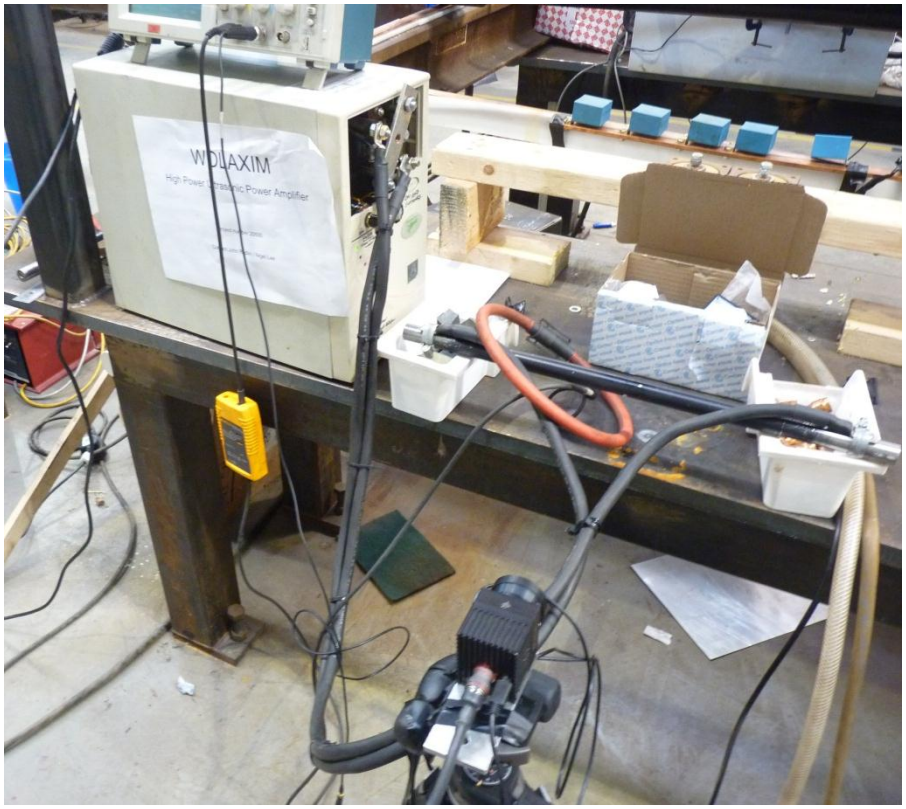

Figure 34 3kW system attached to small test sample by welding wires

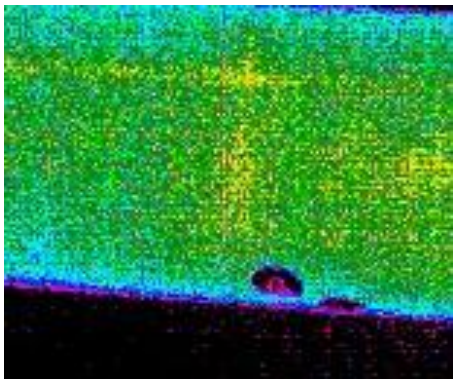

Figure 35 Image of 2mm deep crack at prototype operating frequency

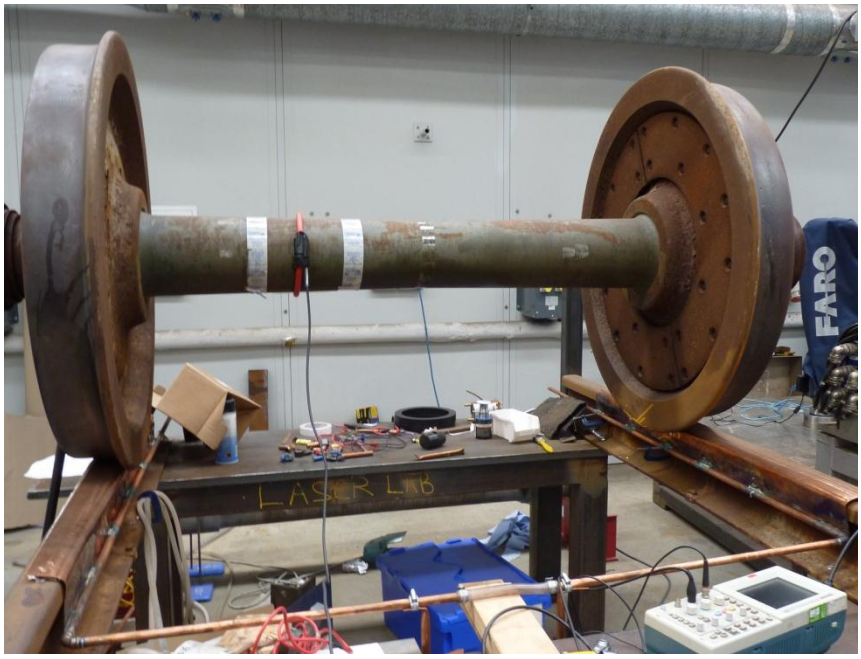

Figure 36 General Arrangement of Experiment

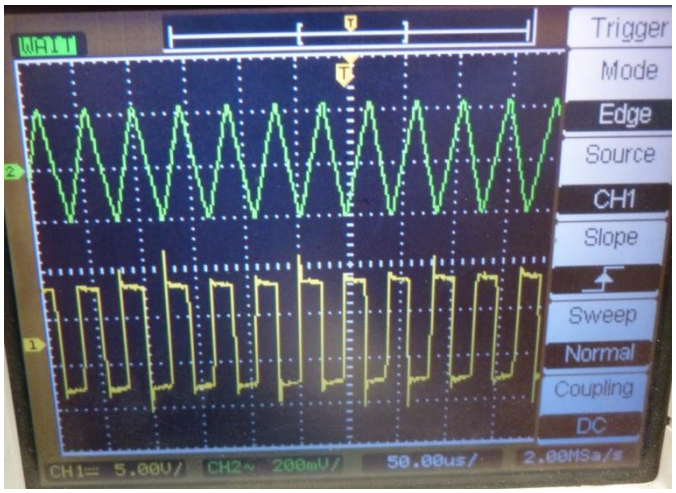

Figure 37 Waveform found for induction system (no resonance)

Figure 38 (a) Initial Feasibility Equipment

Figure 38(b) Prototype 3kW unit

Figure 38(c) Tthe finished prototype 3 phase 25kW unit

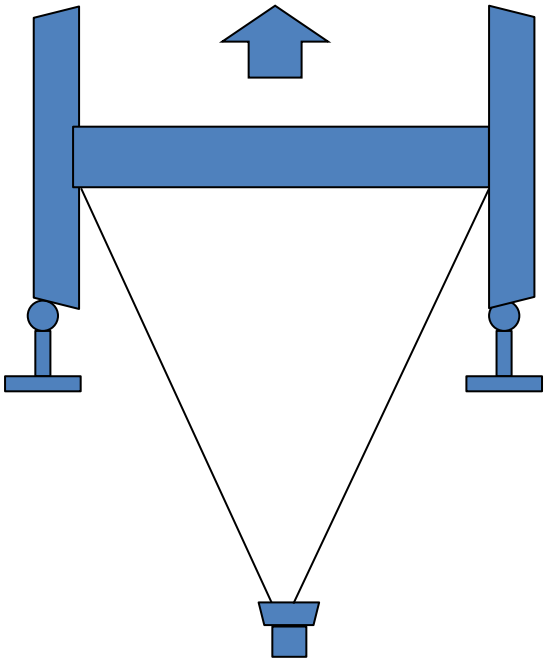

Figure 39 Camera angle to cover axle

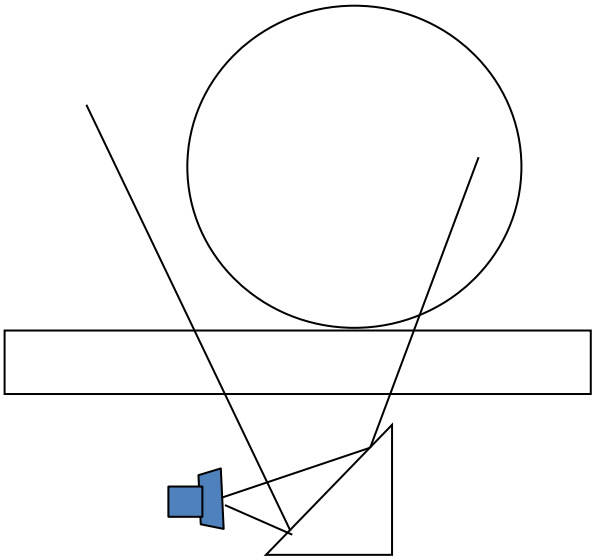

Figure 40 Use of reflector to reduce vertical distance

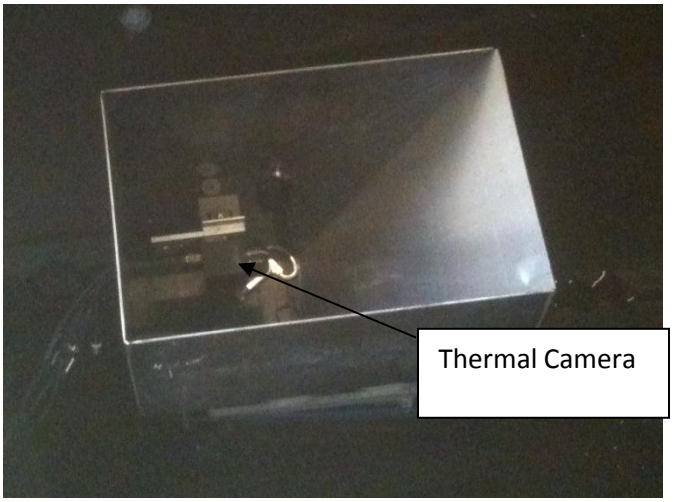

Figure 41 Thermal camera mounted in reflector

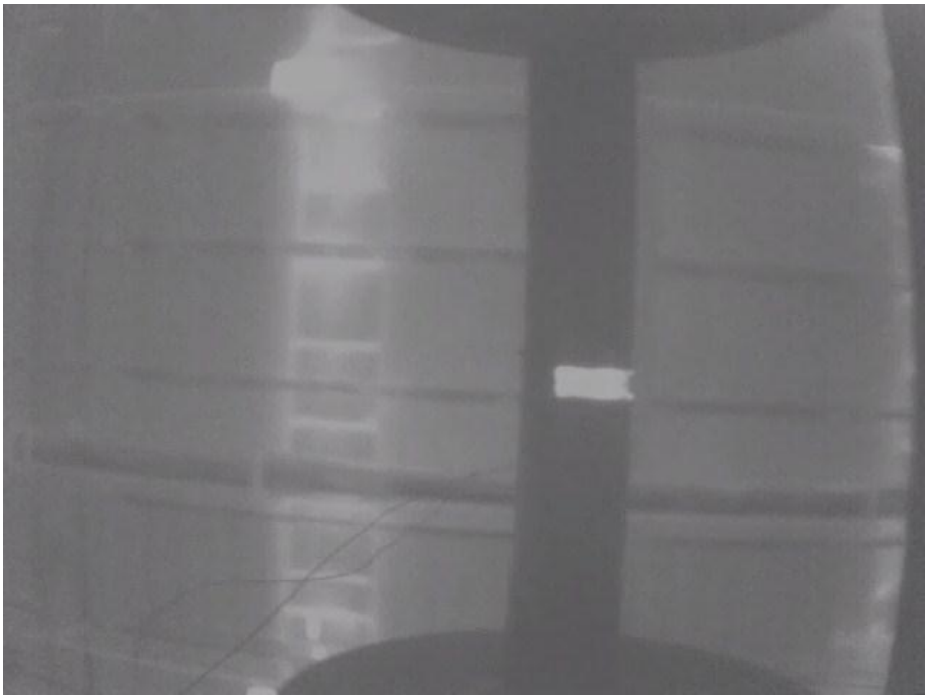

Figure 42 Whole of axle with artificial hotspot around 20mm wide.

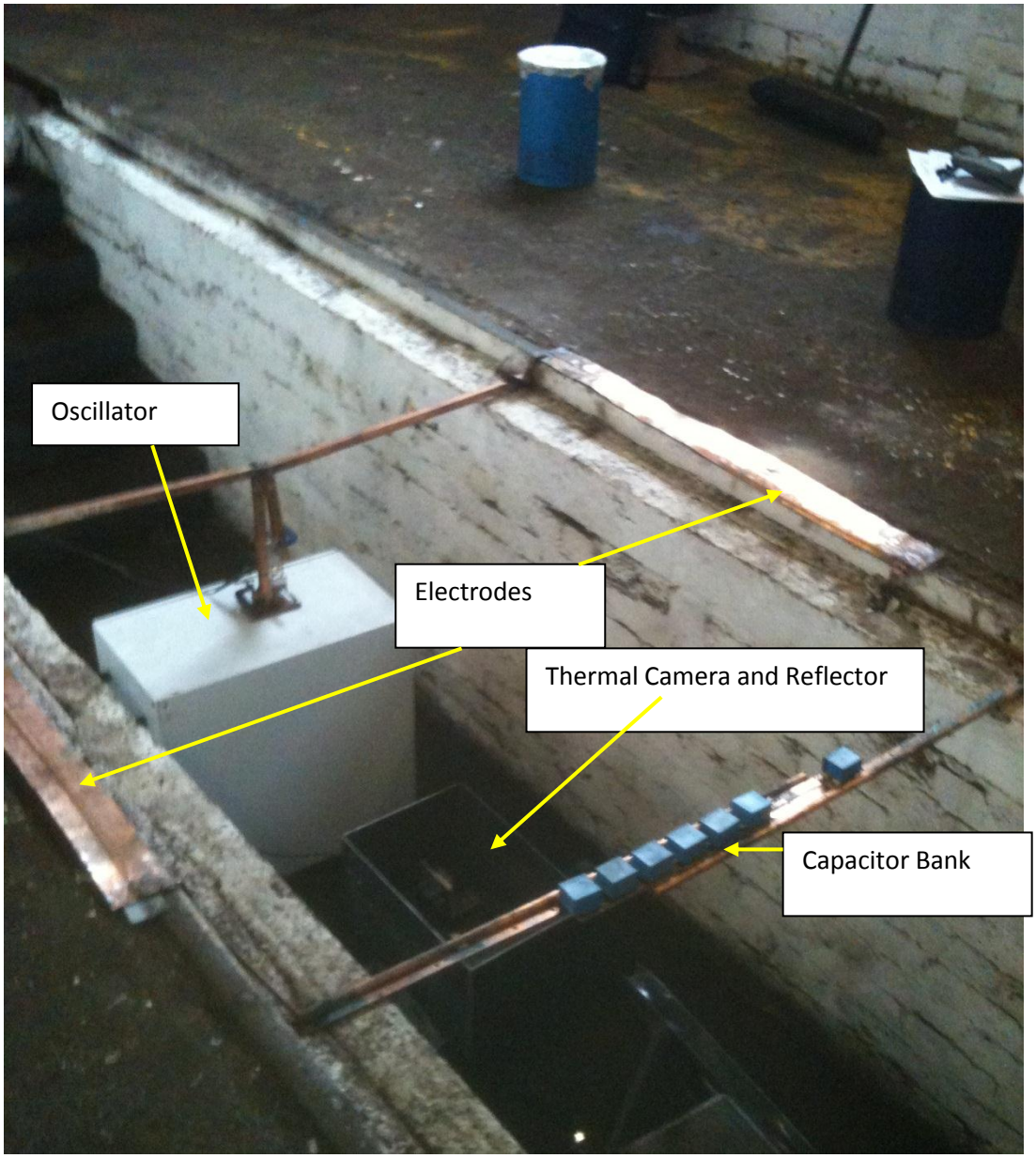

Figure 43 Thermography Field Trials set up

Figure 44 Test Wagon approaching Set Up

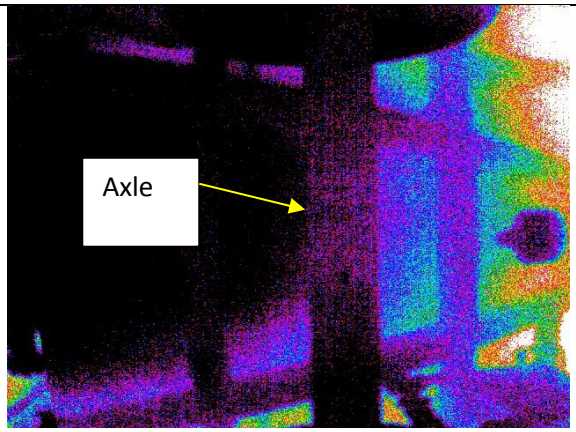

Figure 45(a) Wagon axle at start of heating cycle

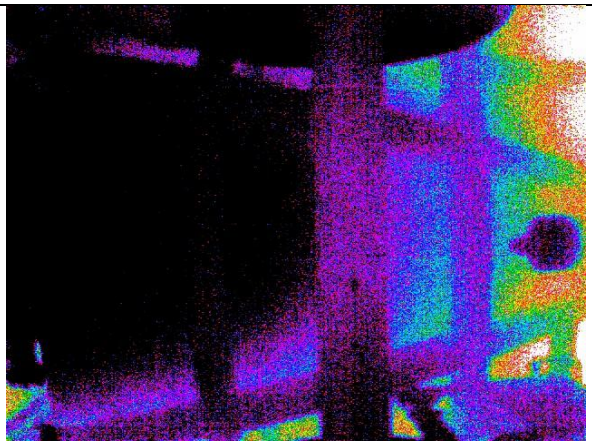

Figure 45(b) Image after 15 secs